ORIGINAL

The Diagnostic Ability of Texture Analysis in MR Imaging for Neurogenic Tumors

Tomoki Matsushita[1], Takayoshi Shinya[1], Toshihiko Nishisho[2], Koichi Sairyo[2], Yoshimi Bando[3], Hisanori Uehara[3], and Masafumi Harada[1]

[1]*Department of Radiology, Tokushima University Hospital, Tokushima, Japan,* [2]*Department of Orthopedics, Tokushima University Hospital, Tokushima, Japan,* [3]*Division of Pathology, Tokushima University Hospital, Tokushima, Japan*

Abstract : Objectives : Malignant peripheral nerve sheath tumors (MPNSTs) are rare neoplasms requiring differentiation from benign neurogenic tumors on diagnostic imaging. We evaluated the diagnostic utility of texture analysis (TA) in distinguishing seven pathologically confirmed MPNSTs from eight schwannomas using magnetic resonance imaging (MRI), including T1- (T1WI) and T2-weighted imaging (T2WI), and apparent diffusion coefficient (ADC) maps. TA's performance was compared with that of conventional approaches using ADC values alone. Methods : Tumors were segmented, and 90 texture features were extracted using LIFEx software. Significantly different features ($p < 0.05$) were identified using the Mann–Whitney *U* test and evaluated through receiver operating characteristic (ROC) analysis. ADC maps were used to measure the minimum, mean, and maximum ADC values, followed by ROC analysis. Results : Two T2WI-based texture features (*neighborhood grey-tone difference matrix Contrast* and *grey-level size zone matrix Grey Level Variance*) demonstrated the highest diagnostic performance (area under the curve = 0.911 [95% confidence interval (CI) : 0.755–1.000]), comparable to the minimum and mean ADC values (area under the curve = 0.898 [95% CI : 0.691–1.000]). Conclusions : TA may help differentiate MPNSTs from schwannomas. T2WI-based TA offers a viable alternative when ADC maps are limited by magnetic susceptibility artifacts. J. Med. Invest. 72 : 367-374, August, 2025

Keywords **:** *Texture analysis, magnetic resonance imaging, schwannoma, malignant peripheral nerve sheath tumor, apparent diffusion coefficient*

INTRODUCTION

Malignant peripheral nerve sheath tumors (MPNSTs) are rare neoplasms originating from Schwann cells, representing 3–10% of all soft-tissue sarcomas (1, 2). In contrast, benign peripheral nerve sheath tumors (BPNSTs) are more prevalent, accounting for 10–12% of benign soft-tissue tumors (2, 3). Differentiating between MPNSTs and BPNSTs is clinically important due to their markedly different prognoses. However, accurate diagnosis can be challenging sometimes due to overlapping clinical and imaging features. Moreover, MPNSTs may arise from pre-existing BPNSTs, including benign schwannomas (4).

While histopathological biopsy remains the diagnostic gold standard, it is associated with risks such as pain, nerve palsy, and potential malignant cell dissemination to visceral organs (5, 6). Consequently, non-invasive imaging plays a pivotal role in the diagnostic workup. One commonly used imaging technique involves assessing apparent diffusion coefficient (ADC) values on diffusion-weighted imaging (DWI). For example, Yun *et al*. demonstrated that mean and minimum ADC values could distinguish between benign and malignant PNSTs, with threshold values of 1.15×10^{-3} mm²/s (area under the curve [AUC] = 0.846 [95% confidence interval (CI) : 0.715–977]) and 0.89×10^{-3} mm²/s (AUC = 0.759 [95% CI : 0.595–0.923]), respectively (3). However, given that PNSTs frequently arise in superficial or paravertebral locations, DWI is susceptible to magnetic susceptibility artifacts, reducing its diagnostic reliability (7, 8).

Received for publication May 26, 2025 ; accepted June 24, 2025.

Address correspondence and reprint requests to Tomoki Matsushita, Department of Radiology, Tokushima University Hospital, Kuramoto-cho, Tokushima, 770-8503, Japan and Fax : +81-886-33-7468.

In recent years, texture analysis (TA) has emerged as a promising image-based technique to extract quantitative features that describe tumor heterogeneity, aiding in diagnosis and prognosis across various tumor types (9, 10). Despite its growing application, no prior study has specifically assessed the diagnostic utility of TA derived from standard routinely acquired MRI sequences, including T1-weighted imaging (T1WI), T2-weighted imaging (T2WI), and ADC maps, in differentiating MPNSTs from BPNSTs.

This retrospective study aimed to evaluate the diagnostic performance of TA applied to T1WI, T2WI, and ADC maps in differentiating MPNSTs from benign schwannomas representing BPNSTs. Additionally, we compare the diagnostic accuracy of TA with that of the conventional ADC value-based method.

PATIENTS AND METHODS

Patient Selection

This single-center retrospective study was approved by the local ethics committee (Approval number : 4376), with all procedures adhering to local data protection regulations and the Declaration of Helsinki.

The inclusion criteria were : (1) a pathological diagnosis of MPNST or benign schwannoma based on biopsy or surgical specimens ; and (2) availability of pre-biopsy or pre-operative 1.5T MRI examinations conducted between April 2013 and April 2022 at our institution, including T1WI, T2WI, and ADC maps suitable for TA.

The exclusion criteria were : (1) inadequate image quality due to low resolution or severe artifacts ; and (2) MRI performed after biopsy or more than 6 months prior to pathological diagnosis. No restrictions were placed on the patient's age, tumor size, or clinical stage.

MRI Data Acquisition

MRI was performed using a 1.5T system (Signa HDxt or Signa Explorer, GE Healthcare, USA). Acquisition parameters were as follows : (a) T1WI : sequence = fast spin echo (FSE) ; repetition time (TR) /echo time (TE) = 391–625/7.3–26.9 ms ; field of view (FOV) = 120 × 120–350 × 350 mm ; matrix = 288 × 192–388 × 388 ; slice thickness = 3–7 mm ; slice gap = 3.5–8 mm ; pixel band width = 81–195 Hz/pixel ; acquisition time = 1 min 48 s–2 min 37 s. (b) T2WI : sequence = FSE ; TR/TE = 2913–5523/93.4–106 ms ; FOV = 120 × 120–350 × 350 mm ; matrix = 288 × 192–320 × 320 ; slice thickness = 3–8 mm ; slice gap = 3.5–10 mm ; pixel band width = 81–244 Hz/pixel ; calculated chemical shift = 0.7–2.5 pixels ; acquisition time = 1 min 30 s–3 min 4 s. (c) DWI : sequence = spin echo-echo planar imaging ; TR/TE = 3315–7239/66.3–93.2 ms ; FOV = 200 × 200–400 × 400 mm ; matrix = 84 × 84–128 × 160 ; slice thickness = 3–6 mm ; slice gap = 3–6 mm ; pixel band width = 81–244 Hz/pixel ; acquisition time = 1 min 39 s–3 min 47 s ; *b*-values = 0 and 700 or 800 s/mm^2.

Texture Feature Analysis

Tumor segmentation and texture feature (TF) extraction were performed using LIFEx version 7.2.0 (IMIV/CEA, Orsay, France) (11). Two diagnostic radiologists (T.M., with 7 years of experience ; and T.S., with 24 years of experience), blinded to the diagnoses, independently delineated regions of interest (ROIs) slice-by-slice on T1WI, T2WI, and ADC maps to generate volumes of interest (VOIs) as large as possible not including outer margin of the tumor to avoid partial volume effects and chemical shift artifacts. Final VOIs were determined by consensus (Fig. 1).

A total of 90 TFs were extracted from each VOI in accordance with the Image Biomarker Standardization Initiative guidelines (12). These included : morphological indices (12 features), intensity histogram parameters (23 features), grey-level co-occurrence matrix (GLCM : 23 features), neighborhood grey-tone difference matrix (NGTDM : 5 features), grey-level run-length matrix (GLRLM : 11 features), and grey-level size zone matrix (GLSZM : 16 features).

TF calculation settings were : (1) spatial resampling to 2.0 × 2.0 × 2.0 mm voxel size and (2) intensity discretization into 64 grey levels between the minimum and maximum values within each VOI (13, 14).

Statistical Analysis

All statistical analyses were performed using EZR version 1.61 (Saitama Medical Center, Jichi Medical University, Japan) (15). The Mann–Whitney *U* test was used to compare continuous variables that did not follow a normal distribution, whereas the Fisher's exact test was used to compare categorical demographic variables. A p-value < 0.05 was considered statistically significant.

Receiver operating characteristic (ROC) curve analysis was conducted for all TFs showing significant differences, and the area under the curve (AUC) was calculated to assess diagnostic performance. As a secondary evaluation, the minimum, mean, and maximum ADC values were measured on the single slice where each tumor size reached the maximum. AUC values for ADC-derived parameters were computed using the same method and statistically compared with those of TFs using DeLong's test (16).

RESULTS

A retrospective review of our institutional database identified 17 patients who met the inclusion criteria. Of these, three were excluded due to a pathological diagnosis being made more than 6 months after MRI acquisition.

The final study cohort comprised 14 patients (4 males, 10 females) with a median age of 57 years (range : 18–81 years). One patient presented with two MPNSTs, resulting in a total of 15 tumors : seven MPNSTs and eight benign schwannomas. The demographic characteristics of the cohort are summarized in Table 1. There was no significant difference in age, sex, and the median maximum tumor size between MPNSTs and schwannomas (p = 0.463, 0.608, and 0.132, respectively).

As T2WI was available for all cases, TA was performed on all 15 tumors. However, T1WI was unavailable in one case each of

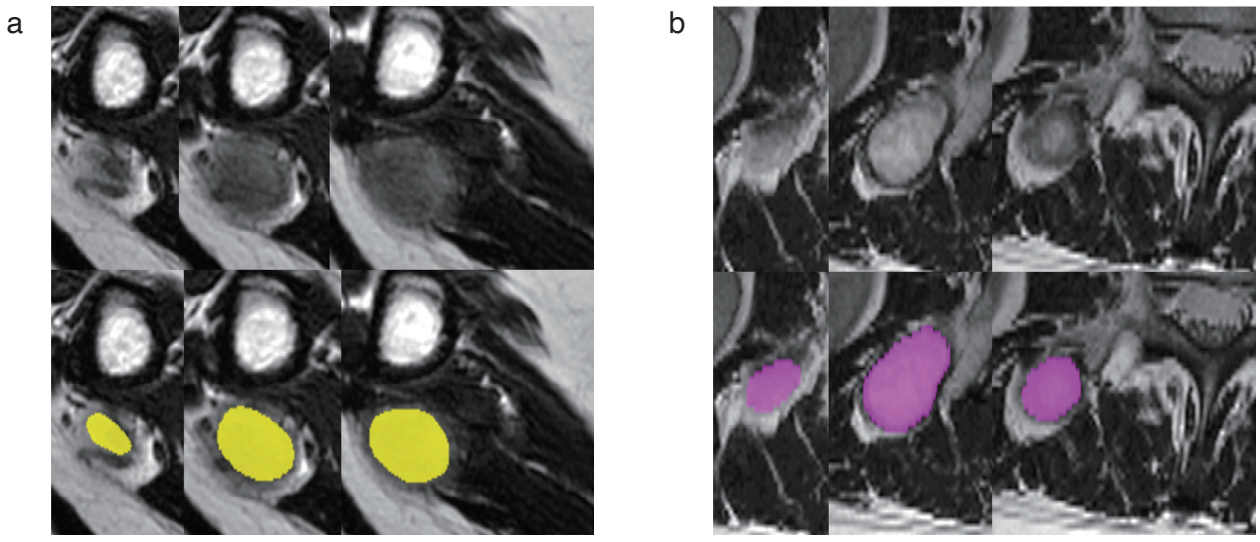

Fig 1. Example images of segmentation for MPNST in the upper limb (a) and schwannoma in the paraspinal space (b). Two diagnostic radiologists independently delineated the regions of interest (ROIs) slice-by-slice on T2-weighted imaging (T2WI), T1-weighted imaging (T1WI), and apparent diffusion coefficient (ADC) maps to generate the volume of interest (VOI).

MPNST and schwannoma, reducing the T1WI-based TA dataset to 13 tumors. ADC maps were unavailable in one schwannoma case, resulting in 14 tumors for ADC map-based TA.

The Mann–Whitney *U* test was applied to the 90 TFs extracted from T1WI, T2WI, and ADC maps. The number of TFs showing statistically significant differences ($p < 0.05$) between MPNSTs and benign schwannomas varied by sequence : 38 for T2WI, 23 for ADC maps, and 1 for T1WI (Table 2). A comprehensive list of significant TFs is provided in the Supplemental Table.

ROC curve analysis was performed for each TF with significant group-wise differences. To streamline reporting, an AUC threshold of 0.87 was used to define high diagnostic accuracy. Table 3 lists the TFs with AUC values exceeding this threshold. The highest AUCs were observed for *T2WI NGTDM Contrast* and *T2WI GZSZM Grey Level Variance*, both achieving an AUC of 0.911 (95% CI : 0.755–1.000).

Among the ADC-derived parameters measured at the single slice where each tumor size reached the maximum, the minimum and mean ADC values showed statistically significant differences between MPNSTs and schwannomas, with AUCs of 0.898 for both (95% CI : 0.691–1.000). In contrast, maximum ADC values did not demonstrate significant differences (Table 4).

Table 1. Demographic and clinical characteristics of the study population

	MPNST	Schwannoma	*p*-value
Tumor	7	8	
Patient (underlying NF-1)	6 (5)	8 (1)	
Median age (years) (range)	53 (18–81)	58 (33–76)	0.463
Sex (male, female)	2, 4	2, 6	0.608
Median maximum tumor size (mm) (range)	59 (26–70)	25 (15–152)	0.132

Table 2. Number of texture features showing significant differences between MPNST and benign schwannoma by feature type

	T2WI	ADC map	T1WI
Morphological indices	None	None	None
Intensity-Histogram parameters	11	11	1
GLCM	17	7	None
NGTDM	2	1	None
GLRLM	3	3	None
GLSZM	5	1	None
Total	38	23	1

Table 3. Texture features with AUC > 0.87 and their corresponding AUC values

T2WI	Features	AUC	95% CI
Intensity-Histogram	Variance	0.875	0.688–1.000
	Mean Absolute Deviation	0.875	0.688–1.000
	Median Absolute Deviation	0.875	0.688–1.000
GLCM	Joint Variance	0.875	0.688–1.000
	Difference Average	0.875	0.660–1.000
	Dissimilarity	0.875	0.660–1.000
	Inverse Difference	0.875	0.660–1.000
	Normalized Inverse Difference	0.875	0.660–1.000
	Inverse Difference Moment	0.875	0.660–1.000
NGTDM	Contrast	0.911	0.755–1.000
GLSZM	Grey Level Variance	0.911	0.755–1.000
ADC maps	Features	AUC	95% CI
Intensity-Histogram	90th Percentile	0.888	0.695–1.000
	Uniformity	0.878	0.634–1.000
GLCM	Joint Average	0.878	0.696–1.000
	Sum Average	0.878	0.696–1.000
	Autocorrelation	0.878	0.696–1.000
GLRLM	Short Run High Grey Level Emphasis	0.878	0.686–1.000

Table 4. Comparison of ADC values between MPNST and benign schwannoma

	MPNST	Schwannoma			
ADC values	Median (range) ($\times 10^{-3}$mm^2/s)	Median (range) ($\times 10^{-3}$mm^2/s)	*p*-value	AUC	95% CI
Minimum	0.94 (0.55–1.20)	1.47 (0.91–1.93)	0.0147	0.898	0.691–1.000
Mean	1.51 (1.23–2.11)	1.95 (1.78–2.40)	0.0111	0.898	0.691–1.000
Maximum	2.09 (1.58–2.96)	2.45 (2.26–2.85)	0.259	0.694	0.371–1.000

Comparative ROC analysis using DeLong's test revealed no statistically significant differences between the two ADC-derived parameters (minimum and mean ADC values) and the two top-performing TFs (*T2WI NGTDM Contrast* and *T2WI GZSZM Grey Level Variance*) (Fig. 2).

DISCUSSION

This study demonstrates that several TFs extracted from T2WI and ADC maps achieve high diagnostic accuracy in distinguishing MPNSTs from benign schwannomas. Among these, *T2WI NGTDM Contrast* and *T2WI GZSZM Grey Level Variance* showed the highest diagnostic performance (AUC = 0.911 [95% CI : 0.755–1.000]).

Both minimum and mean ADC values also differed significantly between MPNSTs and benign schwannomas, each achieving an AUC of 0.898 (95% CI : 0.691–1.000). Notably, DeLong's test revealed no statistically significant difference in diagnostic accuracy between these ADC parameters and the top-performing TFs.

TA is a quantitative imaging technique that uses mathematical descriptors to evaluate image heterogeneity and spatial signal distribution. It can extract information not readily apparent to visual inspection, and has been reported to be potentially relevant to the clinical outcome and pathological characteristics (17). One key application of TA is the non-invasive differentiation between benign and malignant lesions.

A basic component of TA is intensity histogram analysis, which assesses variability and bias in pixel or voxel intensity distribution by dividing values into discrete bins (18). Parameters like kurtosis and skewness derived from these histograms assist in tumor characterization (19). In this study, TFs that measure signal variability — such as variance and uniformity — achieved high AUC values (Table 3). MPNSTs demonstrated lower signal variability than benign schwannomas (Supplemental Table), consistent with histopathological differences : MPNSTs are densely cellular, while schwannomas exhibit a heterogeneous mix of hypercellular *Antoni* A and hypocellular *Antoni* B regions (20). This supports the idea that TA may reflect the underlying tissue pathological architecture, and serve as a potential non-invasive tool for differentiating benign and malignant neurogenic

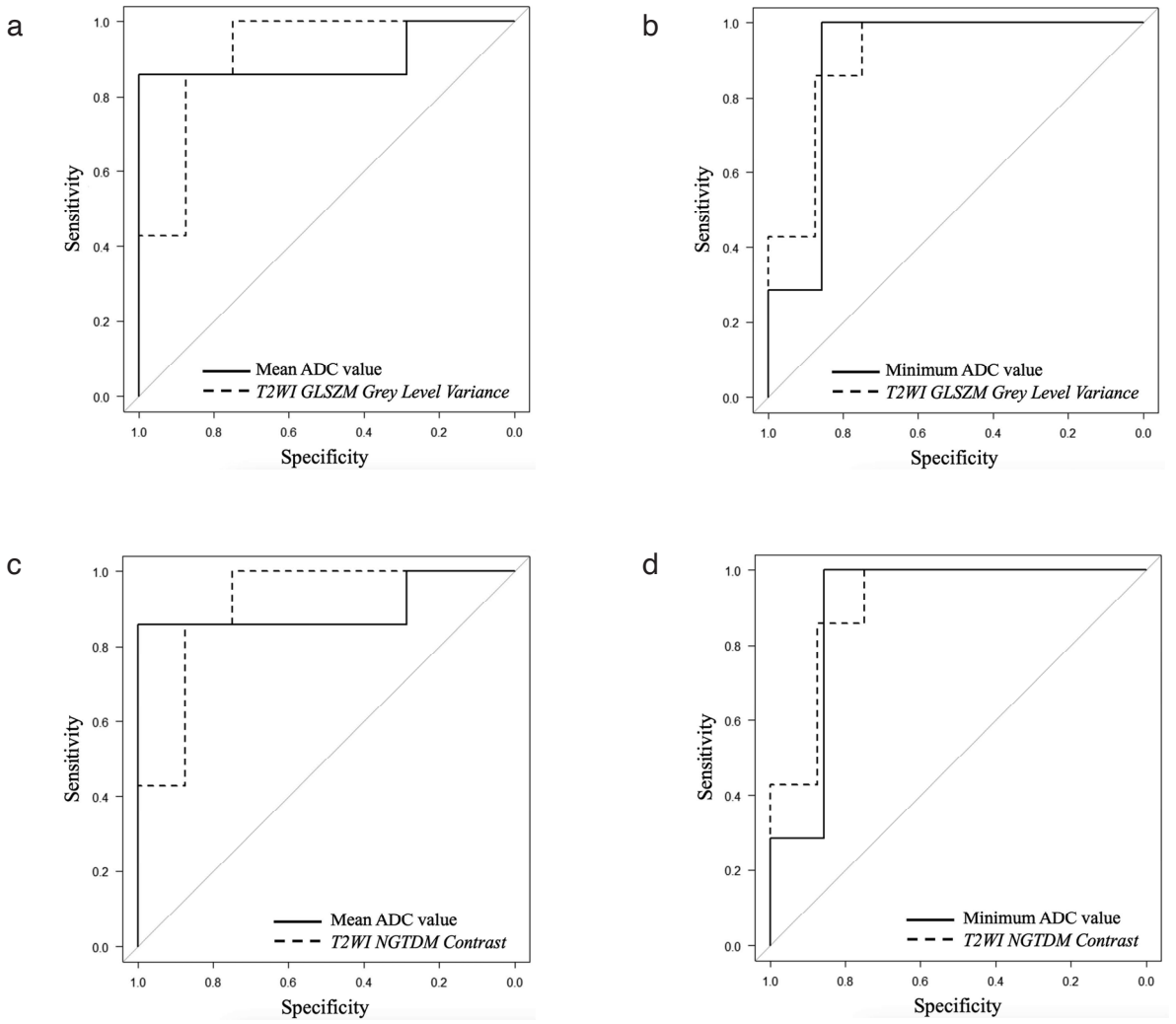

Fig 2. Comparison of receiver operating characteristic (ROC) curves for apparent diffusion coefficient (ADC) values and texture features : (a) mean ADC values vs. *T2WI GLSZM Grey Level Variance*, (b) minimum ADC values vs. *T2WI GLSZM Grey Level Variance*, (c) mean ADC values vs. *T2WI NGTDM Contrast*, and (d) minimum ADC values vs. *T2WI NGTDM Contrast*. DeLong's test showed no statistically significant differences between the ROC curves for any of the paired parameters (all $p > 0.05$).

tumors. However, literature on TA does not provide clear evidence that supports the above hypothesis intertwining pathology and MRI on PNSTs.

A percentile in histogram analysis represents the intensity value below which a given percentage of the data falls. For instance, if the 90th percentile is κ, then 90% of the distribution lies below κ. Thus, a reduced *ADC histogram 90th percentile* under the condition of discretized signal intensity suggests that most internal signals fall within a lower ADC value range when ADC value ranges are comparable in extent, and the measured minimum, mean, and maximum ADC values are lower. Our results demonstrated that *the ADC intensity histogram 90th percentile* was lower in the malignant group (Supplemental Table), consistent with findings from previous studies (21, 22). This may indicate that malignant tumors tend to have lower ADC values and/or exhibit more homogeneous distributions on ADC maps.

When most intensity values cluster within a single bin in a histogram, the uniformity parameter approaches 1 (11). In our study, *ADC intensity histogram uniformity* was closer to 1 in MPNSTs than in benign schwannomas (Supplemental Table). Variance, a measure of signal variability, is calculated as the mean of squared deviations from the average value. In our study, *T2WI intensity histogram variance* was lower in MPNSTs than in benign schwannomas (Supplemental Table). These findings suggest that MPNSTs exhibit more homogeneous intensity distributions on MRI than schwannomas.

GLCM, NGTDM, GLRLM, and GLSZM are advanced textural parameters that assess pixel/voxel intensity distributions within an image. GLCM quantifies the frequency of specific grey-level combinations in adjacent pixels or voxels. GLRLM evaluates grey-level continuity within image stacks, differing from GLCM by analyzing run lengths rather than co-occurrence. GLSZM measures the number of connected pixel/voxel clusters with the same grey level. NGTDM calculates the sum of grey-level differences between a pixel/voxel and its neighboring pixels/voxels within a defined Chebyshev distance (12). In this study, several TFs derived from these advanced textural parameters exhibited significant differences between benign schwannomas and MPNSTs. Specifically, *T2WI GLCM Dissimilarity* and *T2WI GLCM Difference Average* were lower in MPNSTs than in benign schwannomas (Supplemental Table). Dissimilarity and difference average values tend to be lower in uniformly textured lesions (23). Therefore, these findings further suggest that MPNSTs have a more homogeneous signal distribution. This trend aligns with the findings of Ristow *et al*., who reported similar results in their study of neurogenic tumors using T2-weighted turbo spin-echo sequences with fat suppression (spectral attenuated inversion recovery, SPAIR) (10).

Conversely, Qin *et al*. examined the correlation between TFs and glioma grading and found that *ADC GLCM Sum Average* — representing the frequency of specific pixel/voxel pairs with defined spatial relationships — tended to be higher in higher-grade gliomas (24). In contrast, our study found that the *ADC GLCM Sum Average* was lower in MPNSTs. This discrepancy suggests that, while gliomas exhibit increased heterogeneity with malignancy, peripheral neurogenic tumors may display greater homogeneity in their malignant forms. These findings, along with previous studies, indicate that TF values alone may not universally distinguish benign from malignant tumors across all tumor types, as their diagnostic significance varies depending on tumor origin.

T2WI NGTDM Contrast and *T2WI GLSZM Grey Level Variance* had the highest AUC values in our study (each AUC = 0.911 [95% CI : 0.755–1]). The cut-off values were 0.262 for *T2WI NGTDM Contrast* (sensitivity = 1.00, specificity = 0.75) and 125.4 for *T2WI GLSZM Grey Level Variance* (sensitivity = 1.00, specificity = 0.75). *NGTDM Contrast* depends on the dynamic range of grey levels and the spatial frequency of signal variations (25), while *GLSZM Grey Level Variance* measures the variability of zone counts per grey level (12). In the present study, both features had lower values in MPNSTs (Supplemental Table), further supporting the notion that MPNSTs exhibit greater homogeneity than benign schwannomas. Notably, there are other types of MPNSTs besides the classic ones, such as the rhabdomyoblastic, epithelioid, and glandular types and others (26) ; however, the MPNST in our study did not have any pathological features similar to those of these rare subtypes. According to the proportion of these atypical subtypes in study populations, texture analyses may have different diagnostic capacities in discriminating between benign and malignant neurogenic tumors.

In addition to TA, our analysis of ADC values for differentiating MPNSTs from schwannomas showed that both minimum and mean ADC values differed significantly between benign and malignant tumors, with high diagnostic accuracy (AUC = 0.898 for both [95% CI : 0.691–1.000]). The optimal cut-off values were 1.13×10^{-3} mm^2/s for minimum ADC (sensitivity = 0.86, specificity = 0.86) and 1.78×10^{-3} mm^2/s for mean ADC (sensitivity = 0.86, specificity = 0.86). ADC measurement is a conventional and straightforward technique for distinguishing malignant from benign tumors. Notably, Yun *et al*. reported that mean and minimum ADC values are effective in differentiating benign and malignant PNSTs (3). These findings reinforce the utility of ADC maps as a valuable tool in distinguishing MPNSTs from schwannomas.

Furthermore, TA based on T2WI and ADC maps proved useful in differentiating MPNSTs from benign schwannomas on MRI. However, TA did not demonstrate a significant advantage over conventional methods relying solely on ADC values.

PNSTs are often located in subcutaneous or paravertebral regions, where DWI may be affected by artifacts. T2WI generally offers superior artifact resistance and higher image quality compared to DWI (27). In clinical practice, DWI or ADC maps may not always be feasible due to patient-related factors such as claustrophobia or motion artifacts. Given that T2WI is often included in standard MRI protocols, it may provide more detailed anatomical information in addition to offering comparable diagnostic performance to DWI-based TA. Therefore, TA based on T2WI is considered versatile and clinically valuable among the MRI sequences evaluated in this study. Because we studied T2WI without fat suppression, the chemical shift effect must be considered. The calculated shift in this study was ranged from approximately 0.7 to 2.7 pixels for our 1.5T equipment and outer margins of the tumor are not included in each ROIs (VOIs) which would not have a severe influence on the results. However, at higher magnetic field strengths, more attention should be paid to the chemical shift effect.

T1WI-based TA demonstrated fewer significant differences, and its AUC values were generally lower than those obtained from T2WI and ADC maps. This finding is expected, as visual tumor inhomogeneity is more apparent on T2WI and ADC maps than on T1WI. Consequently, when discriminating malignant from benign PNSTs, T1WI has a lower diagnostic priority than T2WI and ADC maps, particularly in cases where MRI examination time is limited.

This study has some limitations. First, the relatively small sample size — driven by the requirement for definitive pathological confirmation — limits the generalizability of our findings. One particular concern is that the MPNSTs in our study were relatively smaller than generally reported. Wasa *et al*. reported a median maximum tumor size of 9.9 cm among 41 MPNSTs (5), whereas in our study, it was 5.9 cm. There might be a bias, given that larger tumors are more likely to have necrosis and can

increase signal heterogeneity. In addition, as mentioned earlier, there are some histopathological variants in MPNST, and we have been unable to perform advanced analysis based on such tumor subtypes. Therefore, future validation in larger cohorts is required. Second, we referred to previous reports on TA in MR imaging to determine analysis settings ; however, optimal ROI and VOI settings for TA have not been fully standardized. Third, reproducibility may be limited, as ROI and VOI delineation were performed manually. Future studies should include larger prospective cohorts and employ automated, computer-aided methods for ROI and VOI segmentation to enhance consistency and reproducibility.

In conclusion, TA demonstrated utility in distinguishing malignant from benign neurogenic tumors in this retrospective study of pathologically diagnosed schwannomas and MPNSTs. However, no significant difference was found between TA and conventional ADC value-based methods, indicating that TA offers comparable diagnostic performance to ADC values. Additionally, TA based on T2WI proved to be a versatile tool for differentiating neurogenic tumors, particularly given that these tumors commonly arise in body surface or paravertebral regions, where T2WI is less susceptible to magnetic susceptibility artifacts than DWI. Furthermore, our findings highlight that MPNSTs exhibited lower signal variability than benign schwannomas, reinforcing the potential role of TA in quantifying tumor heterogeneity and contributing to non-invasive tumor characterization.

CONFLICTS OF INTEREST

The authors declare no conflicts of interest.

ACKNOWLEDGMENTS

The authors would like to express their gratitude to the radiology departments at Tokushima University Hospital for their support in data collection and analysis. We also acknowledge the contributions of the medical imaging technicians who assisted in the interpretation of MRI scans. Additionally, we would like to thank Editage (www.editage.jp) for English language editing.

REFERENCES

1. Yu YH, Wu JT, Ye J, Chen MX : Radiological findings of malignant peripheral nerve sheath tumor : reports of six cases and review of literature. World J Surg Oncol 14 : 142, 2016
2. Debs P, Fayad LM, Ahlawat S : MR neurography of peripheral nerve tumors and tumor-mimics. Semin Roentgenol 57 : 232-240, 2022
3. Yun JS, Lee MH, Lee SM, Lee JS, Kim HJ, Lee SJ, Chung HW, Lee SH, Shin MJ : Peripheral nerve sheath tumor : differentiation of malignant from benign tumors with conventional and diffusion-weighted MRI. Eur Radiol 31 : 1548-1557, 2021
4. Berner EA, Hung YP, Nielsen GP, Lozano-Calderón SA : Malignant peripheral nerve sheath tumors arising from schwannomas : case series and literature review. APMIS 129 : 524-532, 2021
5. Wasa J, Nishida Y, Tsukushi S, Shido Y, Sugiura H, Nakashima H, Ishiguro N : MRI features in the differentiation of malignant peripheral nerve sheath tumors and neurofibromas. AJR Am J Roentgenol 194 : 1568-1574, 2010
6. Pendleton C, Howe BM, Spinner RJ : Percutaneous image-guided biopsy in malignant peripheral nerve sheath tumors. Acta Neurochir (Wien) 163 : 515-519, 2021
7. Xu K, Li Z, Li W, Qiu J, Li H, Li Y, Peng R : Dermatofibrosarcoma protuberans MRI : A preliminary comparison of different sequences. Curr Med Imaging 20 : e15734056307179, 2024
8. Moritani T, Kim J, Capizzano AA, Kirby P, Kademian J, Sato Y : Pyogenic and non-pyogenic spinal infections : emphasis on diffusion-weighted imaging for the detection of abscesses and pus collections. Br J Radiol 87 : 20140011, 2014
9. Scapicchio C, Gabelloni M, Barucci A, Cioni D, Saba L, Neri E : A deep look into radiomics. Radiol Med 126 : 1296-1311, 2021
10. Ristow I, Madesta F, Well L, Shenas F, Wright F, Molwitz I, Farschtschi S, Bannas P, Adam G, Mautner VF, Werner R, Salamon J : Evaluation of magnetic resonance imaging-based radiomics characteristics for differentiation of benign and malignant peripheral nerve sheath tumors in neurofibromatosis type 1. Neuro Oncol 24 : 1790-1798, 2022
11. Nioche C, Orlhac F, Boughdad S, Reuzé S, Goya-Outi J, Robert C, Pellot-Barakat C, Soussan M, Frouin F, Buvat I : LIFEx : a freeware for radiomic feature calculation in multimodality imaging to accelerate advances in the characterization of tumor heterogeneity. Cancer Research 78 : 4786-4789, 2018
12. Zwanenburg A, Leger S, Vallières M, Löck S : Image biomarker standardisation initiative. arXiv preprint, arXiv:1612.07003, 2016
13. Uchida Y, Yoshida S, Arita Y, Shimoda H, Kimura K, Yamada I, Tanaka H, Yokoyama M, Matsuoka Y, Jinzaki M, Fujii Y : Apparent diffusion coefficient map-based texture analysis for the differentiation of chromophobe renal cell carcinoma from renal oncocytoma. Diagnostics (Basel) 12 : 817, 2022
14. Yamada I, Oshima N, Miyasaka N, Wakana K, Wakabayashi A, Sakamoto J, Saida Y, Tateishi U, Kobayashi D : Texture analysis of apparent diffusion coefficient maps in cervical carcinoma : Correlation with histopathologic findings and prognosis. Radiol Imaging Cancer 2 : e190085, 2020
15. Kanda Y : Investigation of the freely available easy-to-use software 'EZR' for medical statistics. Bone Marrow Transplant 48 : 452-458, 2013
16. DeLong ER, DeLong DM, Clarke-Pearson DL : Comparing the areas under two or more correlated receiver operating characteristic curves : a nonparametric approach. Biometrics 44 : 837-845, 1988
17. Corrias G, Micheletti G, Barberini L, Suri JS, Saba L : Texture analysis imaging "what a clinical radiologist needs to know". Eur J Radiol 146 : 110055, 2022
18. Kunimatsu A, Yasaka K, Akai H, Sugawara H, Kunimatsu N, Abe O : Texture analysis in brain tumor MR imaging. Magn Reson Med Sci 21 : 95-109, 2022
19. Kamiya A, Murayama S, Kamiya H, Yamashiro T, Oshiro Y, Tanaka N : Kurtosis and skewness assessments of solid lung nodule density histograms : differentiating malignant from benign nodules on CT. Jpn J Radiol 32 : 14-21, 2014
20. Magro G, Broggi G, Angelico G, Puzzo L, Vecchio GM, Virzì V, Salvatorelli L, Ruggieri M : Practical approach to histological diagnosis of peripheral nerve sheath tumors : An update. Diagnostics (Basel) 12 : 1463, 2022
21. Ozturk M, Polat AV, Selcuk MB : Whole-lesion ADC histogram analysis versus single-slice ADC measurement for the differentiation of benign and malignant soft tissue tumors. Eur J Radiol 143 : 109934, 2021
22. Zhang Z, Song C, Zhang Y, Wen B, Zhu J, Cheng J : Apparent

diffusion coefficient (ADC) histogram analysis : differentiation of benign from malignant parotid gland tumors using readout-segmented diffusion-weighted imaging. Dentomaxillofac Radiol 48 : 20190100, 2019
23. Aghigh A, Cardot J, Mohammadi MS, Jargot G, Ibrahim H, Plante I, Légaré F : Accelerating whole-sample polarization-resolved second harmonic generation imaging in mammary gland tissue via generative adversarial networks. Biomed Opt Express 15 : 5251-5271, 2024
24. Qin JB, Liu Z, Zhang H, Shen C, Wang XC, Tan Y, Wang S, Wu XF, Tian J : Grading of gliomas by using radiomic features on multiple magnetic resonance imaging (MRI) sequences. Med Sci Monit 23 : 2168-2178, 2017
25. de la Luz Escobar M, De la Rosa JI, Galván-Tejada CE, Galvan-Tejada JI, Gamboa-Rosales H, de la Rosa Gomez D, Luna-García H, Celaya-Padilla JM : Breast cancer detection using automated segmentation and genetic algorithms. Diagnostics (Basel) 12 : 3099, 2022
26. Shintaku M, Nakade M, Hirose T : Malignant peripheral nerve sheath tumor of small round cell type with pleomorphic spindle cell sarcomatous areas. Pathol Int 53 : 478-482, 2003
27. Chilla GS, Tan CH, Xu C, Poh CL : Diffusion weighted magnetic resonance imaging and its recent trend-a survey. Quant Imaging Med Surg 5 : 407-422, 2015

Supplemental Table

Texture feature	Median		*p*-value	AUC	95% CI
	MPNST	Schwannoma			
T2WI					
Intensity histogram					
Variance	68.20945622	155.5479137	0.014	0.875	0.688–1.000
Kurtosis	0.528322485	-0.290294287	0.0289	0.839	0.613–1.000
90th Percentile	41	49	0.0314	0.839	0.634–1.000
Interquartile Range	11	17.5	0.0314	0.839	0.615–1.000
Mean Absolute Deviation	6.462239479	10.18849474	0.014	0.875	0.688–1.000
Robust Mean Absolute Deviation	4.656909839	7.571765001	0.0205	0.857	0.688–1.000
Median Absolute Deviation	6.462064444	10.06782864	0.014	0.875	0.688–1.000
Coefficient Of Variation	0.288631358	0.363952139	0.0401	0.821	0.598–1.000
Quartile Coefficient of Dispersion	0.193548387	0.251759834	0.0239	0.857	0.649–1.000
Entropy Log2	5.068672424	5.550036382	0.0205	0.857	0.649–1.000
Uniformity	0.035657851	0.025166488	0.0205	0.857	0.649–1.000
GLCM					
Joint Maximum	0.007167045	0.004619272	0.0289	0.839	0.626–1.000
Joint Variance	61.7751959	137.1519079	0.014	0.875	0.688–1.000
Joint Entropy Log^2	9.454281947	10.13201913	0.0401	0.821	0.598–1.000
Difference Average	5.28254886	7.678845932	0.014	0.875	0.660–1.000
Difference Variance	23.19658687	51.99882234	0.0205	0.857	0.649–1.000
Difference Entropy	9.454281947	10.13201913	0.0401	0.821	0.598–1.000
Sum Variance	204.495719	422.7065395	0.0205	0.857	0.649–1.000
Sum Entropy	9.454281947	10.13201913	0.0401	0.821	0.598–1.000
Angular Second Moment	0.002313776	0.001212564	0.0401	0.821	0.598–1.000
Contrast	54.44649643	111.0484525	0.0205	0.857	0.636–1.000
Dissimilarity	5.28254886	7.678845932	0.014	0.875	0.660–1.000
Inverse Difference	0.29655479	0.224887553	0.014	0.875	0.660–1.000
Normalized Inverse Difference	0.928831177	0.900788344	0.014	0.875	0.660–1.000
Inverse Difference Moment	0.208624886	0.137477049	0.014	0.875	0.660–1.000
Normalized Inverse Difference Moment	0.987428526	0.975826934	0.0205	0.857	0.636–1.000
Cluster Tendency	204.495719	422.7065395	0.0205	0.857	0.649–1.000
Cluster Prominence	143097.5491	595094.8606	0.0205	0.857	0.663–1.000
NGTDM					
Contrast	0.163572275	0.449702212	0.00591	0.911	0.755–1.000
Complexity	4973.513493	7950.451186	0.0289	0.839	0.613–1.000

Texture feature	Median		*p*-value	AUC	95% CI
	MPNST	Schwannoma			
GLRLM					
Short Runs Emphasis	0.949130872	0.973738638	0.0401	0.821	0.564–1.000
Long Runs Emphasis	1.250797679	1.113846629	0.0401	0.821	0.564–1.000
Run Percentage	0.930228612	0.964970443	0.0401	0.821	0.564–1.000
GLSZM					
Large Zone Emphasis	46.65958284	4.468649302	0.0289	0.839	0.590–1.000
Normalized Grey Level Non-Uniformity	0.030059663	0.022759413	0.0205	0.857	0.649–1.000
Zone Percentage	0.400409707	0.623638382	0.0401	0.821	0.564–1.000
Grey Level Variance	93.75421039	156.9999012	0.00591	0.911	0.755–1.000
Zone Size Variance	40.42236654	1.89443391	0.0205	0.857	0.612–1.000
ADC map					
Intensity histogram					
Mean	26.49245331	35.47975078	0.0262	0.857	0.654–1.000
Variance	72.75544318	133.1513099	0.0379	0.837	0.586–1.000
Skewness	0.478205122	-0.470695151	0.0379	0.837	0.586–1.000
Median	26	37	0.0346	0.847	0.638–1.000
90th Percentile	39	50	0.018	0.888	0.695–1.000
Interquartile Range	10	15	0.0342	0.847	0.601–1.000
Mean Absolute Deviation	5.799962972	9.090185867	0.0262	0.857	0.613–1.000
Robust Mean Absolute Deviation	4.053969359	6.608423483	0.0379	0.837	0.586–1.000
Median Absolute Deviation	5.713497823	9.037610619	0.0262	0.857	0.613–1.000
Entropy Log2	4.861029987	5.366512212	0.0262	0.857	0.613–1.000
Uniformity	0.041969157	0.03058006	0.0175	0.878	0.634–1.000
GLCM					
Joint Average	26.09768763	37.63613614	0.0175	0.878	0.696–1.000
Joint Variance	56.0670121	120.0668191	0.0262	0.857	0.613–1.000
Sum Average	52.19537525	75.27227227	0.0175	0.878	0.696–1.000
Sum Variance	195.3480086	355.1661851	0.0262	0.857	0.613–1.000
Angular Second Moment	0.003711337	0.001750221	0.0262	0.857	0.637–1.000
Autocorrelation	722.6962916	1455.914248	0.0175	0.878	0.696–1.000
Cluster Tendency	195.3480086	355.1661851	0.0262	0.857	0.613–1.000
NGTDM					
Complexity	3607.830752	7116.319279	0.0379	0.847	0.586–1.000
GLRLM					
High Grey Level Run Emphasis	795.9334807	1399.096269	0.0262	0.857	0.654–1.000
Short Run High Grey Level Emphasis	745.02301	1360.032472	0.0175	0.878	0.686–1.000
Long Run High Grey Level Emphasis	1078.95118	1577.467712	0.0379	0.837	0.601–1.000
GLSZM					
High Gray Level Zone Emphasis	1061.632921	1309.858447	0.0379	0.837	0.601–1.000
T1WI					
Intensity histogram					
Quartile Coefficient of Dispersion	0.156402737	0.214285714	0.0452	0.845	0.601–1.000